*Human Molecular Genetics, 2008, Vol. 17, No. 14* **2118–2131**
*doi:10.1093/hmg/ddn110*
*Advance Access published on April 7, 2008*

# A sensitized mutagenesis screen identifies *Gli3* as a modifier of *Sox10* neurocristopathy

**Ivana Matera[1,2,†], Dawn E. Watkins-Chow[1,†], Stacie K. Loftus[1], Ling Hou[1], Arturo Incao[1], Debra L. Silver[1], Cecelia Rivas[1], Eugene C. Elliott[1], Laura L. Baxter[1] and William J. Pavan[1,*]**

[1]Genetic Disease Research Branch, National Human Genome Research Institute, National Institutes of Health, Bethesda, MD 20892, USA and [2]Laboratorio di Genetica Molecolare, Instituto G. Gaslini, Genova, Italy

Received January 25, 2008; Revised March 5, 2008; Accepted April 2, 2008

**Haploinsufficiency for the transcription factor *SOX10* is associated with the pigmentary deficiencies of Waardenburg syndrome (WS) and is modeled in *Sox10* haploinsufficient mice ($Sox10^{LacZ/+}$). As genetic background affects WS severity in both humans and mice, we established an *N*-ethyl-*N*-nitrosourea (ENU) mutagenesis screen to identify modifiers that increase the phenotypic severity of $Sox10^{LacZ/+}$ mice. Analysis of 230 pedigrees identified three modifiers, named modifier of *Sox10* neurocristopathies (*Mos1, Mos2* and *Mos3*). Linkage analysis confirmed their locations on mouse chromosomes 13, 4 and 3, respectively, within regions distinct from previously identified WS loci. Positional candidate analysis of *Mos1* identified a truncation mutation in a hedgehog(HH)-signaling mediator, GLI-Kruppel family member 3 (*Gli3*). Complementation tests using a second allele of *Gli3* ($Gli3^{Xt\text{-}J}$) confirmed that a null mutation of *Gli3* causes the increased hypopigmentation in $Sox10^{LacZ/+};Gli3^{Mos1/+}$ double heterozygotes. Early melanoblast markers (*Mitf, Sox10, Dct*, and *Si*) are reduced in $Gli3^{Mos1/Mos1}$ embryos, indicating that loss of GLI3 signaling disrupts melanoblast specification. In contrast, mice expressing only the GLI3 repressor have normal melanoblast specification, indicating that the full-length GLI3 activator is not required for specification of neural crest to the melanocyte lineage. This study demonstrates the feasibility of sensitized screens to identify disease modifier loci and implicates *GLI3* and other HH signaling components as modifiers of human neurocristopathies.**

## INTRODUCTION

Waardenburg syndrome (WS) describes a specific group of neurocristopathies whose phenotypes are primarily caused by melanocyte deficiencies. The features of WS include skin hypopigmentation (leukoderma), pigmentation defects of the choroid and iris, and deafness from loss of inner ear melanocytes. The presence of additional phenotypic anomalies results in four clinically distinct WS types that have been associated with mutations in at least six genes essential for the development of the neural crest (NC), a population of pluripotent cells that differentiates into many functionally diverse cell types. The identified WS genes include paired box gene 3 (*PAX3*), microphthalmia-associated transcription factor (*MITF*), snail homolog 2 (*SNAI2*), endothelin-3 (*EDN3*), endothelin B receptor (*EDNRB*), and Sry-like HMG box 10 (*SOX10*) (1–9). In particular, mutations in *SOX10* have been identified in type II WS (WS2) and type IV WS (WS4), which combine features of WS with absence of enteric neurons (aganglionosis) that is characteristic of Hirschsprung disease (HSCR; OMIM 142623).

*Sox10* is an HMG-box containing transcription factor that is expressed during embryonic development in pre-migratory NC and in a subset of migrating NC cells including those that give rise to the glial and melanocyte lineages (reviewed in 10). The melanocyte precursor cells, melanoblasts, express *Mitf* as they migrate along a dorso-lateral route away from the neural tube. Further differentiation is marked by the subsequent expression

*To whom correspondence should be addressed at: Mouse Embryology Section, Genetic Disease Research Branch, National Human Genome Research Institute, National Institutes of Health, Building 49, Room 4A82, 49 Convent Drive, Bethesda, MD 20892-4472, USA. Tel: +1 3014967584; Fax: +1 3014022170; Email: bpavan@mail.nih.gov
†The authors wish it to be known that, in their opinion, the first two authors should be regarded as joint First Authors.

of the melanosomal protein silver (*Si*, also known as *Pmel17*) and the melanogenic enzyme dopachrome tautomerase (*Dct*) as melanoblasts proceed along their route to the ectoderm where a subset of these colonize the basal epidermis and hair follicles and are readily visible as terminally differentiated melanocytes due to their pigment production (reviewed in 11). Because of its role in multiple NC lineages, *Sox10* is essential for development, and mice carrying heterozygous *Sox10* mutations have NC defects resembling those of WS4, including hypopigmentation and aganglionic megacolon (9,12,13). Similar to humans with WS, the mouse models of WS (14) show phenotypic variability among individuals with the same mutation. Together with WS patients where no mutation has been identified, this phenotypic complexity suggests that additional WS loci remain to be discovered. Mice with *Sox10* mutations offer a unique tool to identify these additional WS loci and explain their mode of action.

In this study we designed a sensitized ENU modifier screen to identify loci that increase the NC defects, specifically white spotting (hypopigmentation), associated with *Sox10* haploinsufficiency. We identified three *Sox10* modifier loci that did not map to known WS loci. At one locus, *Mos1*, a truncation mutation in the transcription factor GLI-Kruppel family member 3 (*Gli3*) was responsible for increased hypopigmentation when present in combination with *Sox10* haploinsufficiency. *Mos1* homozygous embryos show a defect in melanoblast specification, a phenotype that is not recapitulated in embryos expressing a C-terminally truncated form of GLI3 that acts as a repressor. This suggests that the full-length form of GLI3 that acts as a transcriptional activator is not required for melanoblast development. This study demonstrates the feasibility of this sensitized ENU screen to identify modifier loci of *Sox10*, reveals a role for *Gli3* in melanocyte development, and implicates *GLI3* and other hedgehog (HH) signaling components as modifiers of WS.

## RESULTS

### A sensitized mutagenesis screen to identify modifiers of SOX10

A breeding strategy was designed to identify ENU-induced mutations that modify the severity of hypopigmentation in $Sox10^{LacZ/+}$ mice (Supplementary Material, Fig. S1). BALB/cJ male mice were given 3-weekly ENU injections, allowed to recover fertility, and then mated with C57BL/6J females to generate first generation ($G_1$) offspring. $G_1$ males were subsequently mated with $Sox10^{tm1Weg/+}$ heterozygous females (13), herein referred to as $Sox10^{LacZ/+}$, because they contain a targeted disruption of the endogenous *Sox10* locus that drives expression of a β-galactosidase reporter gene from the *Sox10* promoter and predisposes the mice to NC defects. Second generation ($G_2$) offspring were then examined for increased severity of neurocristopathies in $Sox10^{LacZ/+}$ mice, as measured by increased hypopigmentation.

Incorporation of two different inbred strains in this screen made efficient mapping of the BALB/cJ mutagenized allele possible in subsequent crosses to C57BL/6J. Since genetic background could affect the hypopigmentation of the $Sox10^{LacZ/+}$ animals, we performed a control-cross in which non-ENU-treated BALB/cJ males were substituted for the ENU-treated BALB/cJ males. For these and all subsequent crosses, the extent of ventral hypopigmentation was scored according to a standardized scale (0–4), with 0 representing no hypopigmentation and 4 representing the most severe ventral hypopigmentation (Supplementary Material, Fig. S2). The control-cross demonstrated minimal variation in hypopigmentation among $Sox10^{LacZ/+}$ $G_2$ offspring on a BALB/cJ; C57BL/6J mixed genetic background. The control $G_2$ offspring ($N = 111$) received ventral hypopigmentation scores of 0 (79%) or 1 (21%) and dorsal hypopigmentation was never observed. These results showed that genetic background effects from allelic variance between BALB/cJ and C57BL6/J would not interfere with identification of novel, ENU-induced gene mutations affecting pigmentation.

In total, 230 $G_1$ male offspring were generated and at least three litters of $G_2$ offspring from each $G_1$ male were screened for increased hypopigmentation. Seven $G_1$ pedigrees produced one or more $Sox10^{LacZ/+}$ $G_2$ offspring with increased ventral hypopigmentation (score $>2$) accompanied by dorsal hypopigmentation, neither of which was observed in the control cross. In three of these seven $G_1$ pedigrees the observed phenotype was reproducible in subsequent generations, indicating a heritable, mendelian phenotype. These three loci were named modifier of *Sox10* 1, 2 and 3 (*Mos1*, *Mos2*, and *Mos3*) (Fig. 1A).

### *Mos1*, *Mos2* and *Mos3* do not map to previously known WS loci

To determine if *Mos1, 2*, and *3* are due to mutations in genes previously attributed to WS, we mapped these loci. In each pedigree, linkage analysis using a whole genome SNP or SSLP panel was used to test for BALB/cJ alleles that associated with the dominant increase in $Sox10^{LacZ/+}$ hypopigmentation. For mapping *Mos1*, nine mice were used for an initial genome scan (six affected $Sox10^{LacZ/+}$;*Mos1*/+ mice plus three obligate *Mos1*/+ heterozygous carriers). Genotyping of 220 SNPs with distinct alleles in C57BL/6J and BALB/cJ identified a 20 Mb region of proximal mouse Chr 13 where all nine animals had inherited the BALB/cJ allele from the affected founder animal, providing evidence for linkage to markers in this region (0/9 recombinant; $P < 0.01$).

A similar mapping strategy was used to localize *Mos2* and *Mos3* to Chrs 4 and 3, respectively. For *Mos2*, we detected linkage to Chr 4 in a genome scan utilizing 91 SSLP markers to genotype eight affected animals. Subsequent genotyping of affected animals ($N = 31$) in this region localized *Mos2* to 35 Mb region of Chr 4 flanked by markers D4Mit9 (1/31 recombinant; $P < 0.0001$) and D4Mit203 (8/31 recombinant; $P < 0.01$). For *Mos3*, genotyping 408 informative SNPs in five affected animals revealed weak linkage to two regions of the genome. Subsequent genotyping of SSLPs spanning those regions in additional affected animals ($N = 32$) confirmed linkage to a 20 Mb region of Chr 3 flanked by markers D3Mit178 (2/32 recombinant; $P < 0.001$) and D3Mit65 (3/32 recombinant; $P < 0.0001$). The genomic locations of *Mos1, Mos2* and *Mos3* did not overlap with orthologs of WS genes (Fig. 1B), suggesting they are potentially novel WS modifier loci.

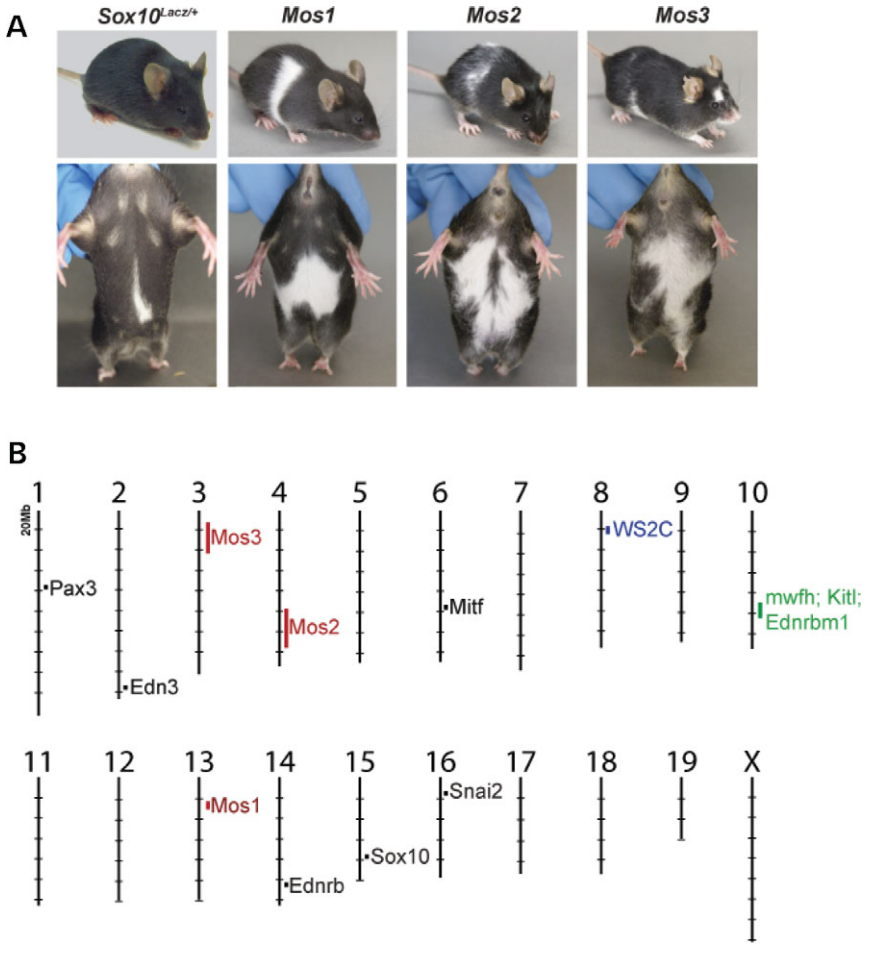


**Figure 1. (A)** Three hypopigmentation phenotypes, *Mos1, Mos2*, and *Mos3*, were identified in an ENU screen that increase the severity of hypopigmentation in $Sox10^{LacZ/+}$ mice. $Sox10^{LacZ/+}$;*Mos1*/+ double heterozygote, *Mos2*/+ heterozygotes, and $Sox10^{LacZ/+}$;*Mos3*/+ double heterozygote individuals are shown after several generations of outcrossing to C57BL/6J. **(B)** The murine genomic locations of *Mos1, 2, 3* map independently from previously identified WS loci. The locations of *Mos1, Mos2*, and *Mos3* (red) are indicated on the mouse physical map relative to the locations of cloned WS genes (black), a regions of conserved synteny for a human WS modifier (WS2C in blue) (61), and a modifier of mouse *Sox10* white forelock hypopigmentation (*mwfh* in green) (62) which overlaps modifiers of mouse $Ednrb^{S}$ hypopigmentation (*Kitl* and *Ednrbm1* in green) (63).

### *Mos1* increases the severity of hypopigmentation in $Sox10^{Lacz/+}$ mice

$Sox10^{LacZ/+}$;*Mos1*/+ affected mice exhibited severe ventral hypopigmentation that often extended onto the dorsal surface forming a belt in the lumbar region (Fig. 2A). To confirm that *Mos1* exacerbated the NC defects in $Sox10^{LacZ/+}$ mice, the penetrance and expressivity of *Mos1* alone and in conjunction with $Sox10^{LacZ/+}$ was analyzed after breeding the *Mos1*/+ founder onto a C57BL/6J background (Fig. 2B and C). Analysis of $G_3$ and $G_4$ offspring showed that with respect to hypopigmentation, *Mos1* alone acts as a semidominant mutation that is not fully penetrant. A portion (37.7%) of heterozygous *Mos1*/+ mice exhibited ventral hypopigmentation ranging in size from 1 to 3 (Fig. 2). Double heterozygous $Sox10^{LacZ/+}$;*Mos1*/+ mice exhibited a significant, synergistic increase in hypopigmentation compared with either single heterozygous *Mos1*/+ or single heterozygous $Sox10^{LacZ/+}$ mice ($P < 0.05$) (Fig. 2). Unlike the majority (75.8%) of $Sox10^{LacZ/+}$ heterozygotes, minimal hypopigmentation (0–1) was not seen in any double heterozygous mice. Ventral hypopigmentation that extended over the dorsal surface to form a belt was seen in 17% of $Sox10^{LacZ/+}$;*Mos1*/+ mice, but was never observed in *Mos1*/+ mice or in $Sox10^{LacZ/+}$ mice. These results indicate that the ENU-induced mutation *Mos1* enhances the melanocyte defects of $Sox10^{LacZ/+}$ mice, acting in synergy with *Sox10* haploinsufficiency to produce more severe NC abnormalities.

### *Mos1* is a novel, nonsense mutation of *Gli3*

Because 95% (84/88) of *Mos1*/+ animals had limb defects resembling the semidominant polydactyly previously identified in *Extratoes* ($Gli3^{Xt}$) (15,16), a classic mouse mutant located on Chr 13, we assessed if the *Gli3* transcription factor was mutated in *Mos1* animals. Genomic DNA from an affected *Mos1*/+ mouse was analyzed by direct sequencing of all coding exons and intron/exon junctions of *Gli3* and compared with sequences of BALB/cJ and C57BL6/J control samples. A single sequence variation was identified in which *Mos1* DNA differed from the parental DNA at a single nucleotide in exon 8 (Fig. 3A).

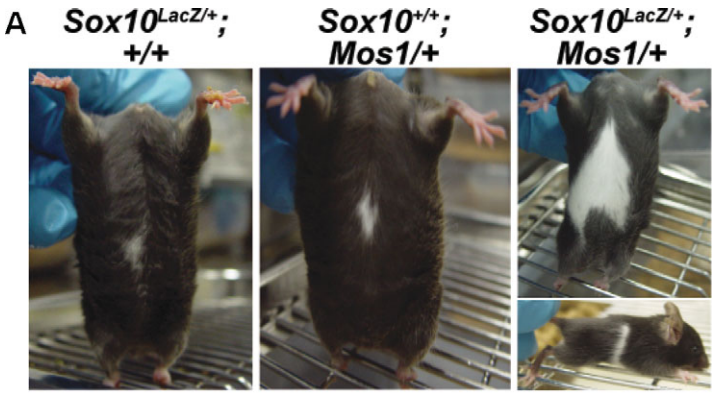


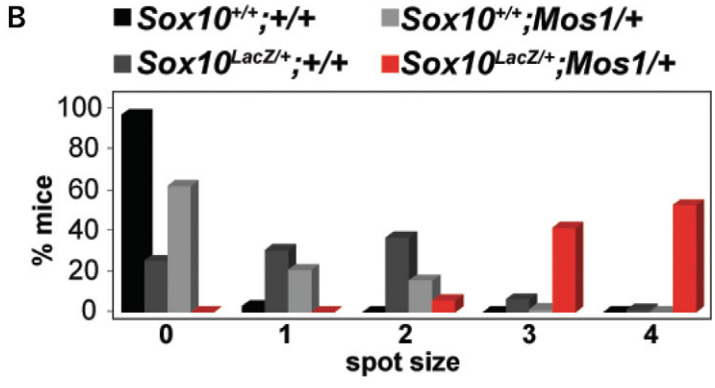


C

| Size Spot | Sox10+/+; +/+ | Sox10LacZ/+; +/+ | Sox10+/+; Mos1/+ | Sox10LacZ/+; Mos1/+ | |
|---|---|---|---|---|---|
| 0 | 101 (97.1%) | 24 (25.3%) | 48 (62.3%) | 0 (0%) | |
| 1 | 3 (2.9%) | 29 (30.5%) | 16 (20.8%) | 0 (0%) | |
| 2 | 0 (0%) | 35 (36.8%) | 12 (15.6%) | 3 (5.7%) | |
| 3 | 0 (0%) | 6 (6.3%) | 1 (1.3%) | 22 (41.5%) | |
| 4 | 0 (0%) | 1 (1.1%) | 0 (0%) | 28 (52.8%) | |
| total | 104 | 95 | 77 | 53 | N=329 |

**Figure 2.** *Mos1* increases hypopigmentation in $Sox10^{LacZ}$ heterozygous mice. **(A)** Heterozygous $Sox10^{LacZ/+}$ mice display a small region of ventral hypopigmentation (left) similar to that observed in heterozygous *Mos1*/+ mice (middle). Double heterozygous $Sox10^{LacZ}$/+; *Mos1*/+ mice exhibit extensive hypopigmentation that frequently extends dorsally as a partial belt (right). **(B, C)** Quantitative data for the extent of ventral hypopigmentation in each of four genotype classes including wild-type ($Sox10^{+/+}$;*Mos1*/+), $Sox10^{LacZ}$ heterozygotes ($Sox10^{LacZ/+}$;*Mos1*+/+), *Mos1* heterozygotes ($Sox10^{+/+}$;*Mos1*/+), and *Sox10*;*Mos1* double heterozygotes ($Sox10^{LacZ/+}$;*Mos1*/+). **(B)** shows a graphical representation of the data, and **(C)** shows the total numbers and percentages within each genotype/phenotype class (total $N = 329$).

The *Mos1* allele carried a nucleotide substitution (1148C>A) predicted to replace Tyr350 with a stop codon (Tyr350Stop; Y350X). Using a real-time PCR genotyping assay, we confirmed that this mutation was not detected in BALB/cJ or C57BL/6J control DNAs and consistently segregated with the *Mos1* phenotype in 100% of animals tested ($N = 130$). The location of the $Gli3^{Mos1}$ nonsense mutation is upstream of the zinc-finger binding domain, suggesting it would disrupt both the activator and repressor forms of GLI3 (Fig. 3B). This is supported by comparison with two other *Gli3* mouse alleles, $Gli3^{Xt\text{-}J}$ and $Gli3^{D699}$, and to published human *GLI3* mutations in Pallister-Hall syndrome (PHS, OMIM 146510) (17) and Greig cephalopolysyndactyly syndrome (GCPS, OMIM 175700) (18). Comparison shows that $Gli3^{Mos1}$ is most similar to $Gli3^{Xt\text{-}J}$ and to GCPS patients with deletions, translocations and point mutations within or upstream of the zinc-finger binding domain (19). Therefore, we propose that $Gli3^{Mos1}$ acts as a loss of function allele.

### Analysis of $Gli3^{Xt\text{-}J}$ confirms that *Mos1* phenotypes result from mutation of *Gli3*

The $Gli3^{Xt\text{-}J}$ allele of *Extratoes* is a deletion that results in phenotypes similar to those in human GLI3-associated disorders,

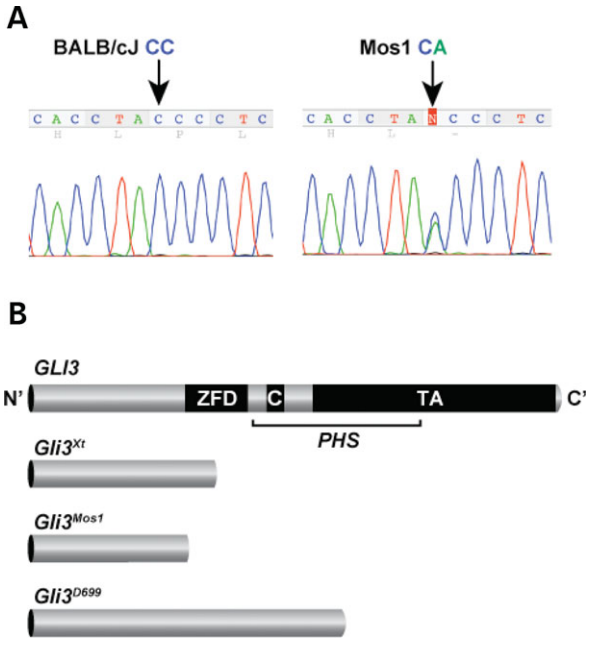


**Figure 3.** A nucleotide substitution in *Mos1* lies in the N-terminal region of the *Gli3* coding sequence. **(A)** Sequencing of BALB/cJ control and *Mos1* heterozygote genomic DNA reveals a C to A substitution at nucleotide position 1148 (arrows) resulting in a nonsense mutation at codon 350 (Tyr350Stop) in the *Mos1* allele. The heterozygous *Mos1* trace shown contains both C (wild-type sequence of BALB/cJ) and A (mutant sequence of *Mos1*) at position 1148. **(B)** Graphic representation of full-length GLI3 protein and 3 truncated proteins resulting from mutant mouse alleles of *Gli3*. The zinc finger domain (ZFD) (34) and proteolytic cleavage site (C) (26) are indicated along with a region of the protein important for transactivation (TA) that spans several fragments independently shown to function in transactivation (64–66). While the $Gli3^{Xt\text{-}J}$ allele results in a truncated protein that lacks the full ZFD and is a loss of function allele, $Gli3^{D699}$ retains the ZFD, and thus functions as a transcriptional repressor. Mutations in the middle third of the human GLI3 gene (bracketed) are predicted to produce truncated functional repressor proteins causing Pallister-Hall syndrome (PHS). The location of the *Mos1* mutation would result in a truncated protein lacking the ZFD, and is predicted to be a loss of function allele similar to $Gli3^{Xt\text{-}J}$, and also to human Greig cephalopolysyndactyly, which is caused by mutations in the human gene that fall outside the bracketed PHS region (19).

including craniofacial defects, brain abnormalities and polydactyly (20). $Gli3^{Xt\text{-}J/Xt\text{-}J}$ homozygotes die *in utero* or at birth with gross polydactyly, multiple craniofacial defects, and exencephaly while $Gli3^{Xt\text{-}J}$ heterozygotes are viable but exhibit an enlarged interfrontal bone and preaxial polydactyly. To determine whether the ENU-induced mutation in *Gli3* causes the *Mos1* phenotype, several analyses were performed to compare the *Mos1* phenotype with the $Gli3^{Xt\text{-}J}$ phenotype. First, to examine if $Gli3^{Mos1/Mos1}$ homozygotes show embryonic lethality similar to that reported for $Gli3^{Xt\text{-}J/Xt\text{-}J}$, $Gli3^{Mos1/+}$ mutant mice were intercrossed and genotype classes were examined at weaning. Of 24 progeny recovered at weaning, no homozygotes were identified, indicating that the $Gli3^{Mos1}$ mutation is lethal in homozygotes (0/24 offspring; $P < 0.005$). Next, allelism was assessed by genotyping the viable offspring from a complementation cross between mice heterozygous for each allele ($Gli3^{Mos1/+}$ X $Gli3^{Xt\text{-}J/+}$). $Gli3^{Mos1}/Gli3^{Xt\text{-}J}$ compound heterozygotes were never observed at weaning (0/32 offspring; $P < 0.01$), confirming that $Gli3^{Mos1}$ and $Gli3^{Xt\text{-}J}$ are allelic. Finally, heterozygous $Gli3^{Xt\text{-}J/+}$ mice were mated with $Sox10^{LacZ/+}$ mice, and offspring of each genotype class was analyzed for hypopigmentation. Similar to $Sox10^{LacZ/+};Gli3^{Mos1/+}$ mice, $Sox10^{LacZ/+};Gli3^{Xt\text{-}J/+}$ double heterozygous mice showed a significant increase in the penetrance and severity of hypopigmentation compared with $Gli3^{Xt\text{-}J/+}$ or $Sox10^{LacZ/+}$ heterozygous animals (Fig. 4). Taken together these results show that *Gli3* is functionally disrupted in *Mos1* mice causing the increased hypopigmentation observed in $Sox10^{LacZ/+};Gli3^{Mos1/+}$ mice.

### *Gli3* deficiency disrupts development of $Sox10^{LacZ}$-expressing cells

To further assess the effects of the $Gli3^{Mos1}$ mutation as a modifier of NC defects, $Sox10^{LacZ/+};Gli3^{Mos1/+}$ mice were crossed to either $Sox10^{LacZ/+};Gli3^{Mos1/+}$ or $Gli3^{Mos1/+}$ mice, and embryos were collected for morphological and histological analyses. At E11.5, we observed craniofacial anomalies including microphthalmia and malformation of the diencephalon and mesencephalon in $Sox10^{LacZ/+};Gli3^{Mos1/Mos1}$ embryos (Fig. 5). These phenotypes are consistent with those in $Sox10^{LacZ/+};Gli3^{Xt\text{-}J/Xt\text{-}J}$ embryos and what has been previously described for $Gli3^{Xt\text{-}J/Xt\text{-}J}$ embryos (15). The patterning of the $Sox10^{LacZ}$-expressing dorsal root ganglia (DRG), sympathetic ganglia and cranial ganglia, visualized by LacZ staining, appeared unaffected in $Sox10^{LacZ/+};Gli3^{Mos1/Mos1}$ embryos as compared with $Sox10^{LacZ/+}$ control embryos (Fig. 5). In contrast, there was a striking reduction in the number of $Sox10^{LacZ}$-expressing melanoblasts within the medial lateral trunk of $Sox10^{LacZ/+};Gli3^{Mos1/Mos1}$ embryos (Fig. 5D–I). Notably, in regions lacking $Sox10^{LacZ}$-expressing melanoblasts, there were ectopically located $Sox10^{LacZ}$-expressing cells positioned dorsal to the DRG that were larger than $Sox10^{LacZ}$-expressing melanoblasts (Fig. 5E and H, arrowheads). $Sox10^{LacZ/+};Gli3^{Xt\text{-}J/Xt\text{-}J}$ mutant embryos also exhibited reduced $Sox10^{LacZ}$-expressing melanoblasts and large ectopic $Sox10^{LacZ}$-expressing cells in their trunks, confirming that these phenotypes resulted from GLI3 deficiency (Fig. 5F and I).

### *Mos1* mutant embryos show dramatic reduction in early stage melanoblasts

To further investigate the reduction in melanoblasts observed in the mid-trunk of $Sox10^{LacZ/+};Gli3^{Mos1/Mos1}$ mutants, we next evaluated expression of the early melanoblast markers *Mitf* and *Si* in homozygous $Gli3^{Mos1/Mos1}$ embryos (Fig. 6). In E11.5 wild-type embryos, numerous melanoblasts were present in the head, cervical region, tail and trunk. As was observed with $Sox10^{LacZ}$ expression, *Mitf*- and *Si*-positive melanoblasts were reduced in number in the mid-trunk of mutant $Gli3^{Mos1/Mos1}$ embryos compared with wild-type embryos (Fig. 6). These data demonstrate that GLI3 deficiency alone disrupts normal trunk melanoblast specification. No ectopic expression was observed for *Mitf* or *Si*, suggesting that the ectopic *Sox10*-positive cells in $Sox10^{LacZ/+};Gli3^{Mos1/Mos1}$ embryos (Fig. 5) were not specified melanoblasts, but instead represent other SOX10-expressing NC derivatives, potentially melanoblast precursors.

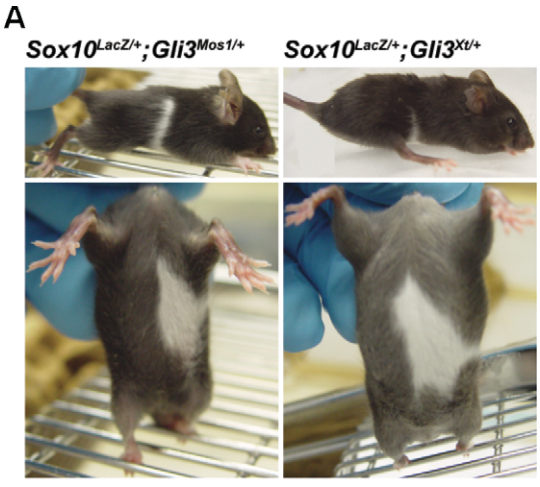


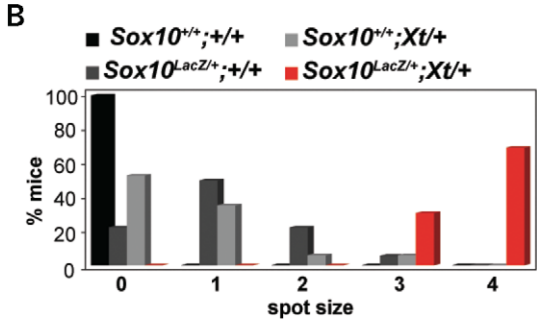


C

| Size Spot | Sox10+/+; +/+ | Sox10LacZ/+; +/+ | Sox10+/+; Xt/+ | Sox10LacZ/+; Xt/+ | |
|---|---|---|---|---|---|
| 0 | 23 (100%) | 4 (22.2%) | 9 (52.9%) | 0% | |
| 1 | 0% | 9 (50.0%) | 6 (35.3%) | 0% | |
| 2 | 0% | 4 (22.2%) | 1 (5.9%) | 0% | |
| 3 | 0% | 1 (5.6%) | 1 (5.9%) | 4 (30.8%) | |
| 4 | 0% | 0% | 0% | 9 (69.2%) | |
| total | 23 | 18 | 17 | 13 | N=71 |

**Figure 4.** The *Gli3*$^{Xt\text{-}J}$ allele increases hypopigmentation in *Sox10*$^{LacZ}$ heterozygous mice similar to the ENU mutation *Mos1*, showing that *Mos1* is a *Gli3* allelic variant. **(A)** Double heterozygous *Sox10*$^{LacZ/+}$;*Gli3*$^{Xt\text{-}J/+}$ mice show enhanced ventral and dorsal hypopigmentation (right) very similar to *Sox10*$^{LacZ/+}$;*Mos1*/+ mice (left). **(B, C)** Representative data for ventral hypopigmentation phenotypes for each four genotype classes including wild-type (*Sox10*$^{+/+}$;*Gli3*$^{+/+}$), *Sox10*$^{LacZ}$ heterozygous mutants (*Sox10*$^{LacZ/+}$;*Gli3*$^{+/+}$), *Gli3*$^{Xt\text{-}J}$ heterozygous mutants (*Sox10*$^{+/+}$;*Gli3*$^{Xt\text{-}J/+}$), and double heterozygotes (*Sox10*$^{LacZ/+}$;*Gli3*$^{Xt\text{-}J/+}$). **(B)** Shows a graphical representation of the data, and **(C)** shows the total numbers and percentages within each genotype/phenotype class (total $N = 71$).

To determine if the melanoblast deficiency in GLI3-deficient embryos persists beyond E11.5, the effect of the *Gli3*$^{Mos}$ mutation on the melanoblast lineage was examined at multiple developmental stages. For this the *Tg*(*Dct-LacZ*) line of transgenic mice was used in which the *Dct* promoter drives expression of LacZ in melanoblasts, caudal embryonic DRG, and the telencephalon (21–23). As with other melanoblast markers, the *Gli3*$^{Mos1/Mos1}$;*Tg*(*Dct-LacZ*) embryos demonstrated a severe reduction in melanoblast numbers in the mid-trunk region, throughout the ventral and dorsal surfaces at E11.5 (Fig. 7). This deficiency persisted through E14.0 and E16.0, at which time *Gli3*$^{Mos1/Mos1}$;*Tg*(*Dct-LacZ*) embryos presented with a large ventral region devoid of melanoblasts that extended around the lumbar trunk area (Fig. 7G–J). Heterozygous *Gli3*$^{Mos1/+}$;*Tg*(*Dct-LacZ*) embryos were less severely affected than their homozygous littermates and at E16.0 exhibited a small ventral region devoid of melanoblasts (data not shown), consistent with the appearance of a small white spot of ventral hypopigmentation in a subset of heterozygous animals (Fig. 2A).

In addition to melanoblasts, LacZ is expressed in the retinal pigment epithelium (RPE), DRG, and telencephalon of *Tg*(*Dct-LacZ*) embryos. In *Mos1* mutant embryos, we did not observe any changes in the *Tg*(*Dct-LacZ*) expression in the RPE or DRG, but *Tg*(*Dct-LacZ*) expression was absent in the telencephalon of *Gli3*$^{Mos1/Mos1}$;*Tg*(*Dct-LacZ*) embryos in comparison with *Gli3*$^{+/+}$;*Tg*(*Dct-LacZ*) embryos at E11.5, E14.0 and E16.0 (Fig. 7, E16.0 data not shown). The loss of *Tg*(*Dct-LacZ*) expression in the telencephalon is not due to altered *Sox10* expression in *Gli3*$^{Mos1/Mos1}$;*Tg*(*Dct-LacZ*) embryos, as *Sox10*$^{LacZ/LacZ}$;*Tg*(*Dct-LacZ*) embryos, which lack any functional SOX10, retain expression of *Tg*(*Dct-LacZ*) in the telencephalon (data not shown). The loss of the normal dorsal *Tg*(*Dct-LacZ*) expression in the *Gli3*$^{Mos1/Mos1}$;*Tg*(*Dct-LacZ*) telencephalon is consistent with the ventralization of the telencephalon previously reported in *Gli3* mutants (24,25).

## GLI3 deficiency does not prevent melanocyte differentiation

As *Gli3* deficiency results in lethality, it was not clear whether GLI3 is required for the end stages of melanocyte differentiation such as melanin pigment production. To address this, NC cultures grown from E9.5 wild-type, *Gli3*$^{Mos1/+}$ ($N = 3$), and *Gli3*$^{Mos1/Mos1}$ ($N = 3$) embryos were grown in media supportive of melanocyte differentiation for 14 days. These cultures can be highly variable, however, it was clear that regardless of the genotype, all cultures generated large numbers of differentiated, highly pigmented melanocytes indicating that NC derived from *Gli3*$^{Mos1/+}$ and *Gli3*$^{Mos1/Mos1}$ embryos can produce fully differentiated melanocytes (Supplementary Material, Fig. S3). Additionally, skin was isolated from *Gli3*$^{Mos1/Mos1}$ embryos and grafted onto nude mice. Skin grafts from both wild-type ($N = 2$) and *Gli3*$^{Mos1/Mos1}$ embryos ($N = 3$) produced pigmented hairs indicating that GLI3-deficient melanoblasts are able to terminally differentiate, enter hair follicles and produce pigmented hairs (Supplementary Material, Fig. S3).

## GLI3 repressor is sufficient for melanoblast specification

Because GLI3 can act as either a transcriptional activator or repressor in response to HH signaling (26), we sought to determine which GLI3 function was active during melanoblast development and therefore responsible for the modulation of the Sox10 haploinsufficiency defects. Our data strongly suggests that *Gli3*$^{Mos1}$ is a null allele predicted to lack both the GLI3 activator and the GLI3 repressor. Therefore, we used *Gli3*$^{D699}$ (*Gli3*$^{tm1Urt}$) mice that express a C-terminally truncated form of GLI3 that acts only as a transcriptional repressor (27), and analyzed *Gli3*$^{+/+}$, *Gli3*$^{D699/+}$ and *Gli3*$^{D699/D699}$ embryos for *Si* expression at E12.5. Unlike the severe reduction in melanoblasts in the trunk of *Gli3*$^{Mos1/Mos1}$ embryos (Fig. 6 D and H), melanoblast numbers in

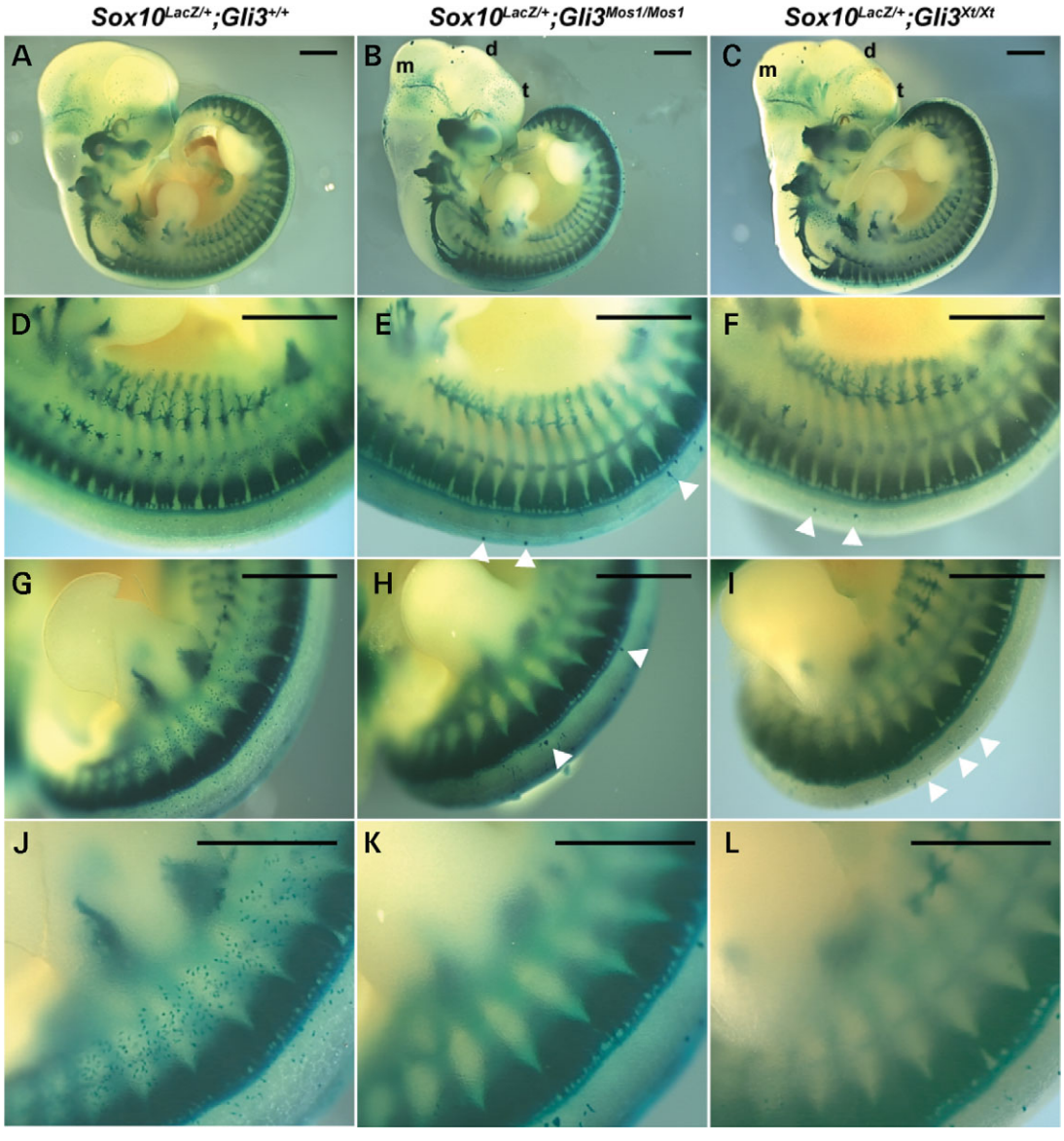


**Figure 5.** *Sox10*$^{LacZ}$ expression in *Gli3*$^{Mos1/Mos1}$ embryos reveals reduced melanoblasts and ectopic *Sox10*$^{LacZ}$-expressing cells. *Sox10*$^{LacZ/+}$;*Gli3*$^{+/+}$ **(A, D, G, J),** *Sox10*$^{LacZ/+}$;*Gli3*$^{Mos1/Mos1}$ **(B, E, H, K),** and *Sox10*$^{LacZ/+}$;*Gli3*$^{Xt\text{-}J/Xt\text{-}J}$ **(C, F, I, L)** embryos at E11.5 after X-gal staining. Shown are lateral (A–C) views of E11.5 embryos and the corresponding trunk (D–F) and hind limb regions (G–L). Microphthalmia, as well as malformation of the mesencephalon (m), diencephalon (d) and telencephalon (t) are visible in *Sox10*$^{LacZ/+}$;Gli3$^{Mos1/Mos1}$ (B) and *Sox10*$^{LacZ/+}$;Gli3$^{Xt\text{-}J/Xt\text{-}J}$ embryos (C). The *Sox10*$^{LacZ}$-expressing sympathetic, cranial and DRG appeared unaffected in *Sox10*$^{LacZ/+}$;Gli3$^{Mos1/Mos1}$ (B) and *Sox10*$^{LacZ/+}$;Gli3$^{Xt\text{-}J/Xt\text{-}J}$ (C) embryos as compared with *Sox10*$^{Lacz/+}$ control embryos (A). Ectopic *Sox10*$^{LacZ}$-expressing cells adjacent to the neural tube in *Sox10*$^{LacZ/+}$;Gli3$^{Mos1/Mos1}$ (E, H) and *Sox10*$^{LacZ/+}$;Gli3$^{Xt\text{-}J/Xt\text{-}J}$ (F, I) embryos are indicated by arrowheads. The number of *Sox10*$^{LacZ}$-expressing melanoblasts was reduced in *Sox10*$^{LacZ/+}$;*Gli3* $^{Mos1/Mos1}$ (E, H, K) and *Sox10*$^{LacZ/+}$;Gli3$^{Xt\text{-}J/Xt\text{-}J}$ (F, I, L) embryos within the medial lateral trunk region as compared with *Sox10*$^{Lacz/+}$ control embryos (D, G, J).

*Gli3*$^{D699/D699}$ homozygote embryos ($N = 4$) appeared grossly normal compared with *Gli3*$^{D699/+}$ heterozygote ($N = 2$) and *Gli3*$^{+/+}$ wild-type embryos ($N = 2$) (Fig. 8). The normal melanoblast specification in *Gli3*$^{D699/D699}$ embryos suggests that the GLI3 repressor promotes melanoblast specification in the absence of full-length GLI3 activator.

## DISCUSSION

In *Sox10* haploinsufficient mice and other disease models, quantitative trait loci (QTL) analysis has been a successful approach to map a number of loci that modify the severity of disease traits, however, identification and confirmation of the causative sequence variation is labor intensive and has only been completed for a small number of mapped QTLs (28). Additionally, recent data suggest that variation among the classical inbred strains is limited and not evenly distributed throughout the genome (29), thus leaving large regions of the genome without the sequence diversity needed to be screened using current QTL methodologies. One way to increase the repertoire of genetic variation that can be tested for modifier effects is to introduce genome wide mutations into genetic


**Figure 6.** GLI3 deficiency disrupts melanocyte specification in the trunk. Shown are lateral views of E11.5 embryos after whole-mount *in situ* hybridizations of wild-type **(A, B, E, F)** and $Gli3^{Mos1/Mos1}$ **(C, D, G, H)** embryos with probes specific for the melanoblast markers *Mitf* **(**A–D**),** and *Si* **(**E–H**).** $Gli3^{Mos1/Mos1}$ embryos show *Mitf* and *Si* expression patterns similar to wild-type embryos in the head and in cervical and tail regions **(**A, C, E, G**).** However, in the trunk region between forelimb and hind limb, $Gli3^{Mos1/Mos1}$ embryos show very few melanoblasts **(**D, H**)** as compared with wild-type embryos **(**B, F**).**

crosses where the phenotype of interest has been well characterized, thus allowing potential modifier effects for every locus in the genome to be screened. Historically, this type of mutagenesis screen to identify enhancers and suppressors of phenotypes has been extremely successful in lower model organisms (30) and more recently applied in mice to identify factors involved in selective biological processes (31,32). Indeed, these mutagenesis screens have some distinct advantages over QTL analysis for the identification of specific sequence variations that modify a phenotype of interest (33) including the relative ease with which the causative sequence variation can be identified.

In this paper, we present a sensitized mutagenesis screen to identify candidate genes for human neurocristopathies. Using this dominant screen we identified three loci that increased the severity of neurocristopathy in *Sox10* haploinsufficient mice and have mapped these loci to regions not previously attributed to known WS loci. By including *Sox10* haploinsufficiency in the screen, we can identify mutations with no heterozygote phenotype on their own, which otherwise could only be detected with an additional generation of breeding ($\sim$10 weeks in mice) that is required for a traditional three-generation recessive screen. In addition, our screen retains mutations that could be missed in a three-generation recessive screen due to embryonic lethality, which was in fact observed for all 3 of the loci reported here. The use of two different inbred strains in the screen eliminated the outcrossing required to map loci, thus allowing us to quickly determine if our phenotypes are caused by mutations in novel loci or represent mutations in previously identified NC development and disease genes.

One of the pedigrees identified in our ENU screen, *Mos1*, showed semidominant hypopigmentation and polydactyly

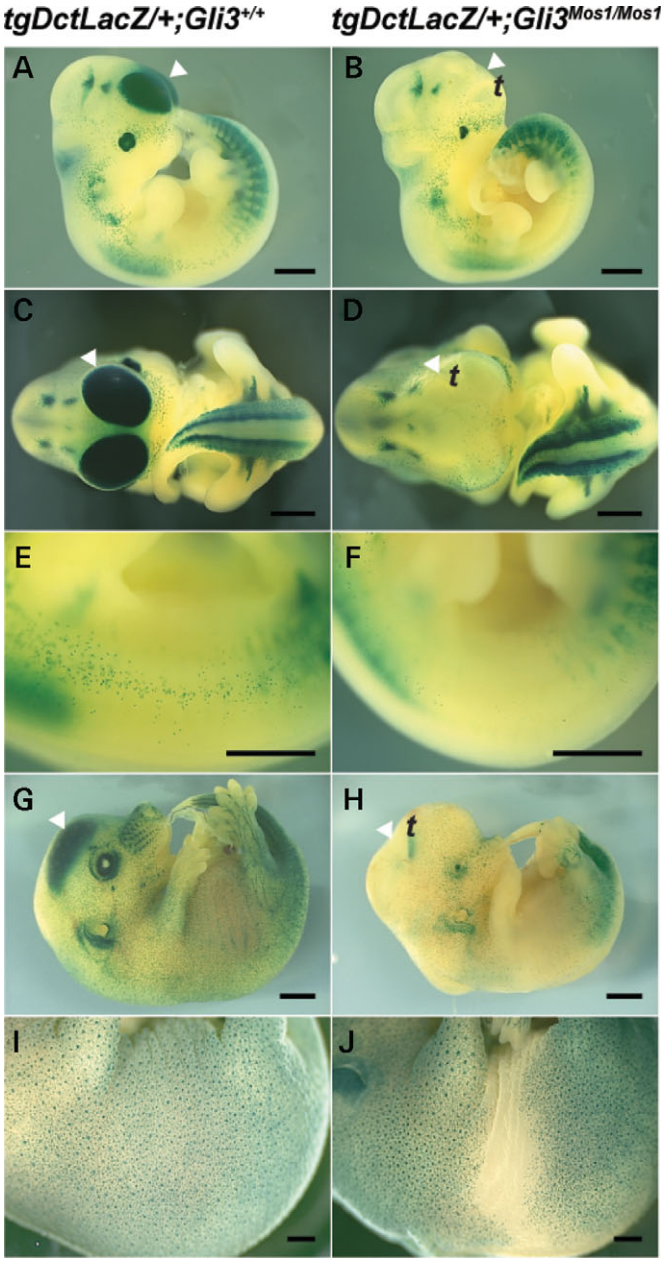


**Figure 7.** *Tg*(*Dct-LacZ*) expression reveals reduction of melanoblasts in *Gli3*$^{Mos1/Mos1}$ embryos. Lateral **(A, B, E–J)** or frontal **(C, D)** views of Gli3$^{+/+}$; *Tg*(*Dct-LacZ*) (A, C, E, G, I) and Gli3$^{Mos1/Mos1}$;*Tg*(*Dct-LacZ*) (B, D, F, H, J), embryos after X-gal staining. The trunk region extending from the ventral to the dorsal surface of *Gli3*$^{Mos1/Mos1}$ embryos shows a severe reduction of melanoblast numbers at E11.5 (B, F) and E14.0 (H) compared with *Gli3*$^{+/+}$; *Tg*(*Dct-LacZ*) embryos at E11.5 (A, E), and E14.0 (G). Lateral view of E16.0 Gli3$^{Mos1/Mos1}$; *Tg*(*Dct-LacZ*) embryo (J) shows a reduction of melanoblast numbers of the ventral and lumbar trunk regions compared with *Gli3*$^{+/+}$; *Tg*(*Dct-LacZ*) E16.0 embryos (I). Arrowheads (A–D, G and H) point toward *Tg*(*Dct-LacZ*) expressing cells of the telencephalon (t). A complete absence of *Tg*(*Dct-LacZ*) expression was noted in the telencephalon (t) of *Gli3*$^{Mos1/Mos1}$;*Tg*(*Dct-LacZ*) embryos at E11.5 (B, D) and E14.0 (H) compared with *Gli3*$^{+/+}$;*Tg*(*Dct-LacZ*) embryos (A, C at E11.5; G at E14.0).

and resulted in homozygous embryonic lethality. The extent of hypopigmentation was significantly increased in *Mos1*/+; *Sox10*$^{LacZ/+}$ double heterozygotes compared with mice carrying heterozygous mutations in either single gene suggesting a synergistic interaction between the two loci. Subsequent linkage and candidate gene analysis identified a causative point mutation in *Gli3*. We showed that a previously published null allele of *Gli3*, *Gli3*$^{Xt\text{-}J}$, had similar effects on pigmentation and survival. Additionally, a complementation test done by intercrossing *Gli3*$^{Xt\text{-}J/+}$ and *Gli3*$^{Mos1/+}$ mice failed to produce any viable compound heterozygous mice carrying both mutations, thus providing strong evidence that the stop mutation identified in *Gli3*$^{Mos1}$ results in a functionally null allele that is responsible for the hypopigmentation in the *Mos1* mice. Double heterozygous mice carrying mutations in both *Sox10* and *Gli3* show a significant increase in hypopigmentation compared with the *Sox10*$^{LacZ/+}$ heterozygous mice. In particular, double heterozygous *Sox10*$^{LacZ/+}$;*Gli3*$^{Mos1/+}$ mice exhibit extensive ventral hypopigmentation that can extend over the dorsal surface to form a belt. Using *Mitf, Si, Dct*$^{LacZ}$ and *Sox10*$^{LacZ}$ expression analysis, we showed that *Gli3* deficiency results in a vast reduction of melanoblasts in the trunk.

*Gli3* is a member of the GLI family of C2H2-type zinc finger transcription factors whose members are vertebrate homologs of the *Drosophila* Cubitus interruptus (Ci) gene (34). GLI family members mediate the final stages of HH signaling and their regulation of HH target genes plays an important role during embryogenesis (reviewed in 35). The timing and location of *Gli3* expression in the dorsal neural tube overlaps with where NC cells form (20,36), consistent with a role for GLI3 in specification of NC derivatives. However, the reduction in melanoblast specification in *Gli3*$^{Mos1/Mos1}$ embryos is unlikely to result from an overall reduction of NC, since DRG and sympathetic ganglia appear relatively normal in these regions. Our observation that GLI3 deficiency does not impair later stages of melanocyte differentiation is consistent with an early role for GLI3 during specification of the melanocyte lineage. Interestingly, melanoblast specification outside the trunk region of *Gli3*$^{Mos1/Mos1}$ embryos was not noticeably reduced. This embryonic phenotype is consistent with the phenotype in *Sox10*$^{LacZ/+}$; *Gli3*$^{Mos1/+}$ adult animals where hypopigmentation is limited to the trunk. This region-specific effect on melanoblast specification could be reflective of normal, wild-type melanoblast distribution, where lower melanoblast numbers are seen in the mid-trunk region (21,22,37). Alternatively, there could be independent pathways that compensate for the loss of GLI3 in regions outside the trunk. Collectively, our data provides strong evidence supporting a role for *Gli3* in early specification of the melanocyte lineage.

During development, GLI3 can act as either a transcriptional activator or repressor, and HH signaling regulates this dual activator/repressor function. In the presence of HH, full-length GLI3 activates target genes, while in the absence of HH, posttranslational cleavage of the C-terminus of GLI3 produces an N-terminal form of GLI3 that acts as a repressor (26) (reviewed in 38 and 39). Given that the NC is induced at the dorsal neural tube in a region with low HH activity, we predict that the GLI3 repressor would be the main GLI3 protein product involved in melanoblast specification. In support of this hypothesis, *Gli3*$^{D699/D699}$ mutant embryos, which specifically express only the C-terminally truncated GLI3 repressor

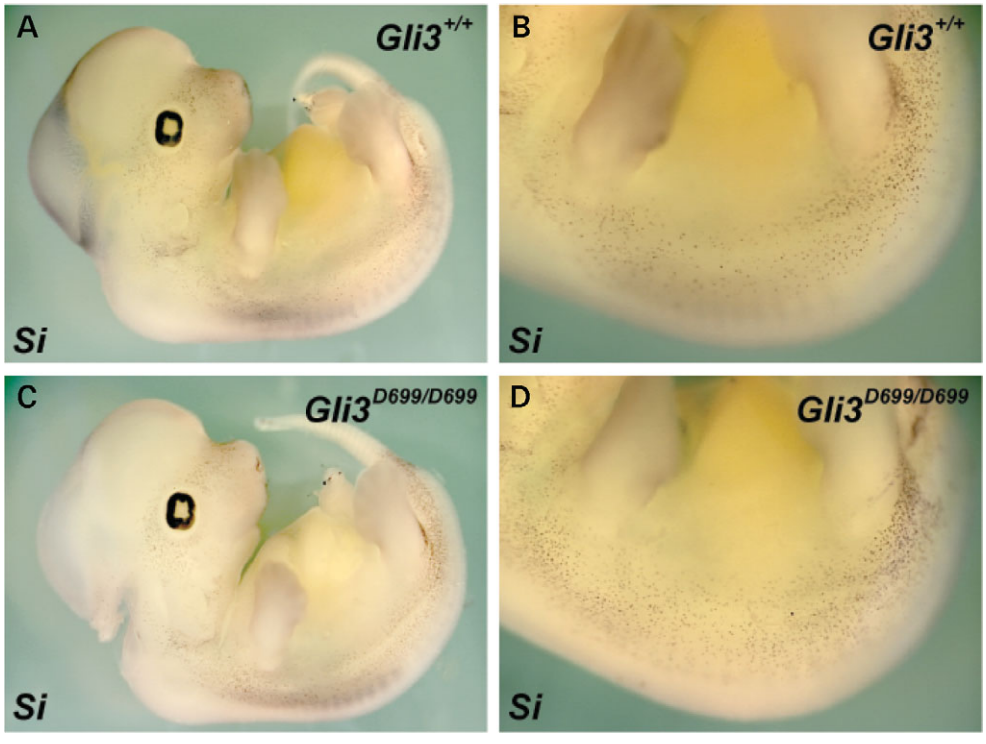


**Figure 8.** GLI3 repressor is sufficient for melanoblast specification in the trunk. Shown are lateral views of E11.5 embryos after whole-mount *in situ* hybridizations of wild-type **(A, B)** and $Gli3^{D699/D699}$ **(C, D)** embryos with probes specific for the melanoblast marker *Si*. $Gli3^{D699/D699}$ embryos show *Si* expression patterns similar to wild-type embryos. We did not observe a drastic reduction in trunk melanoblasts as was observed in $Gli3^{Mos1/Mos1}$ embryos (Fig. 6) that lack both GLI3 activator and repressor function.

(27), had normal numbers of trunk melanoblasts. These results show that the repressor form of GLI3 promotes melanoblast specification, and suggest that a low level of HH signaling is required for normal melanoblast specification.

The precise mechanism through which the GLI3 repressor acts to facilitate melanoblast specification remains to be determined. Because *Sox10* interacts with a number of genes during melanocyte development, including *Mitf* (40–43) and components of the wingless-related MMTV integration site (Wnt) signaling pathway (44,45), the genetic interaction we observe between *Gli3* and *Sox10* mutants could be mediated through these other pathways rather than a direct interaction with *Sox10*. Recent work reveals that canonical Wnt signaling may directly activate *Gli3*, thereby helping to establish dorsal ventral patterning within the spinal cord (46). Interestingly, the GLI3 repressor has been shown to inhibit canonical Wnt signaling by physically interacting with and antagonizing active forms of β-catenin (47). Thus, *Gli3* appears to be both a target of and a regulator of canonical Wnt signaling. The careful balance of HH and Wnt signaling was shown to affect neuronal subtypes within the developing spinal cord (46) suggesting that perhaps interactions between the HH and Wnt signaling cascades could also play a role in melanocyte progenitor cell fate. Wnt signaling is known to influence the proliferation and specification of melanocyte precursors (48–52), and it is possible that loss of GLI3 repressor in $Gli3^{Mos1/Mos1}$ mutants perturbs the balance of HH and Wnt signaling, resulting in a ventralization of cell fate that affects the melanocyte lineage.

As a well-established downstream target and mediator of Wnt signaling (53–55), *Mitf* provides an intriguing direct target for GLI3 repression within the melanocyte lineage. However, a preliminary search for GLI3 binding sites did not identify any highly conserved GLI3 binding sites within the *Mitf* promoter suggesting that the GLI3 repressor acts indirectly to regulate *Mitf* expression. While it is likely that GLI3 interacts with a number of target genes during NC lineage specification, *Foxd3* is a promising candidate for a GLI3 target and we hypothesize that this binding could indirectly regulate *Mitf* expression. *Fox* genes have been implicated in mediating HH signaling in craniofacial NC derivatives (56) and the zebrafish *foxd3* directly binds the *mitfa* promoter, thereby repressing transcription and inhibiting *mitfa*-positive melanoblast specification (57). Therefore it is possible that in $Gli3^{Mos1/Mos1}$ mutants, *Foxd3* expression is deregulated, thus disrupting melanoblast specification. While significant future work remains to determine the mechanism through which the GLI3 repressor affects melanoblast specification, our findings clearly implicate GLI3 as a participant in these networks and uncover a new role for GLI3 in the melanocyte lineage.

In conclusion, we have identified three loci that act as modifiers for *Sox10*-dependent melanocyte defects, increasing both penetrance and severity of the defects in $Sox10^{LacZ/+}$ heterozygous mice. We have shown that one of these loci is a mutation in *Gli3* and have demonstrated the phenotype caused by a reduction in normal *Gli3* gene dosage is significantly exacerbated by a reduction in *Sox10* gene dosage

(*Sox10*$^{LacZ/+}$ mice), suggesting that the two genes cooperate, directly or indirectly, during specification of the melanocyte lineage. These data highlight the role of *Gli3* signaling in melanocyte development, and predict the importance of future studies investigating the role of *GLI3* and/or *SOX10* in other human disorders that combine digit and melanocyte defects.

## MATERIALS AND METHODS

### Mouse husbandry

BALB/cJ and C57BL/6J inbred mouse strains were purchased from The Jackson Laboratory. Engineered mice with a LacZ cassette replacing the endogenous *Sox10* locus (*Sox10*$^{LacZ}$ or *Sox10*$^{tmWeg}$) (13) were obtained on a mixed genetic background and maintained at NHGRI by crossing to C57BL/6J. The *Gli3*$^{Xt\text{-}J}$ mice that carry a spontaneous mutation in *Gli3* were purchased from The Jackson Laboratory (stock B6.C3-*Gli3*$^{Xt\text{-}J}$/J) and maintained at NIH by crossing to C57BL/6J. *Gli3*$^{tm1Urt}$, herein referred to as *Gli3*$^{D699}$ mice, were provided by Ulrich Ruther (27). All other mice described in the ENU screen and embryology studies were bred and housed in an NHGRI animal facility according to NIH guidelines. For genotyping, genomic DNA was prepared from tail biopsies or yolk sacs using a PUREGENE DNA purification kit (Gentra Systems, Inc., Minneapolis, MN, USA) according to the manufacturers instructions. Noon on the day of vaginal plug observation was designated E0.5 for timed pregnancies.

### ENU injections

ENU was prepared and injections carried out as previously described (58). Briefly, *N*-ethyl-*N*-nitrosourea (ENU) (Sigma; St. Louis, MO, USA) was dissolved at 100 mg/ml in 95% ethanol and then diluted to 5 mg/ml in a sterile phosphate/citrate buffer (0.1 M dibasic sodium phosphate, 0.05 M sodium citrate, pH 5.0). A spectrophotometer reading at a wavelength of 398 nm was used to confirm the ENU concentration, and BALB/cJ male mice were given weekly intraperitoneal injections of 0.1 mg/g of body weight for three consecutive weeks. Mice were allowed to recover for 8 weeks post-injection and loss of fertility was confirmed by mating with C57BL/6J females. Five males that lost and subsequently regained fertility ($G_0$) were bred to C57BL/6J females beginning at 12 weeks post-injection. In total, 230 resulting first generation progeny ($G_1$) were crossed to *Sox10*$^{LacZ/+}$ mice and all subsequent offspring ($G_2$) were observed at weaning for hypopigmentation that extended beyond the ventral surface.

### Quantitation of hypopigmentation

To quantitate the extent of ventral hypopigmentation in *Sox10*$^{LacZ/+}$ mice in $G_2$ mice bred from non-mutagenized BALB/cJ males, the ventral surface of mice was photographed and the area of hypopigmentation was quantitated as a proportion of the total ventral surface area. Analysis was performed using the public domain NIH Image software developed at the U.S. National Institutes of Health and freely available (http://rsb.info.nih.gov/nih-image). Once the extent of hypopigmentation was shown to be consistent in the $G_2$s from the BALB/cJ and C57BL/6J mixed genetic background, all mice bred for this study were assigned a numerical score of 0–4,with 1 representing the smallest spots of visible hypopigmentation, to quantitatively represent the extent of ventral hypopigmentation observed.

### Genetic mapping and sequencing

All three *Mos* loci were mapped using only affected animals for analysis. For the full genome scans, affected *Mos1 and Mos3* mice were genotyped on the Illumina platform for SNPs polymorphic between the BALB/cJ and C57BL/6J parental strains used in this study (Brigham Women's Hospital, Harvard University). Affected *Mos2* mice were genotyped at polymorphic SSLP markers (CIDR, The Johns Hopkins University). A standard $\chi^2$ test was used to analyze backcross data for linkage (59) using the number of recombination events per number of meiotic opportunities for each marker. For *Mos1*, the linkage to Chr 13 was consistent with data from a previous genome scan where suggestive but not significant linkage to proximal Chr 13 was detected with fewer markers (91 SSLP markers).

Sequencing of *Gli3* was carried out using standard techniques to PCR amplify each exon and surrounding splice sites from genomic DNA for sequence analysis (Harvard Partners Healthcare Center for Genetics and Genomics, Harvard Medical School). The sequence of an affected *Mos1*/+ heterozygote was compared with the sequence of the parental inbred strains to identify a single nucleotide change on the ENU-treated BALB/cJ chromosome.

### Genotyping

Taqman® MGB probes (Applied Biosystems, Foster City, CA, USA) were designed across the *Gli3*$^{Mos1}$ mutation (1148C>A) specific for the wild-type BALB/cJ allele (VIC-CTTCACCTACCCCTCC) and the ENU induced mutant allele (FAM-CTTCACCTAACCCTCC). PCR reactions were carried out in 1X Taqman® Universal PCR Master Mix (Applied Biosystems) containing 900 nM of each primer (TCCACAGCCCTGCATTGAG and AGGATC TGTTGATGCATGTGAAGAG), and 200 nM of each allele-specific probe. Cycling conditions were 2 min at 50°C, 10 min at 95°C followed by 40 cycles of 92°C for 15 s, 60°C for 1 min. Relative quantitation of the two alleles was determined in an end-point assay.

Genotyping of the *Gli3*$^{D699}$ colony knock-in allele was confirmed by Thymidine kinase (TK) positive PCR amplification with TkFOR GATGCGGCGGTGGTAATGAC and TkREV TGTGTCTGTCCTCCGGAAGG primers amplifying a 295 bp PCR product. Presence of the wild-type *Gli3* allele for the *Gli3*$^{D699}$ colony was detected using primers Gli3-int13for: GGCCCAAACATCTACCAACACATA and Gli3-int14rev: CTGGCCACACTGAAAGGAAAAGAA, amplifying a 541 bp product. Genotype determination for *Gli3*$^{Xt\text{-}J}$ colony was performed using primers XtJ580F: TACCCCAG CAGGAGACTCAGATTAG and XtJ580R: AAACCCGTGG CTCAGGACAAG, amplifying a 590 bp Xt allele and primers C3F: GGCCCAAACATCTACCAACACATAG and

C3R: GTTGGCTGCTGCATGAAGACTGAC, amplifying a 193 bp wild-type allele.

*Sox10*$^{LacZ}$ and *Tg*(*Dct-LacZ*) genotyping was performed by PCR amplification of the *LacZ* cassette as previously reported (23).

### Beta-galactosidase staining

Embryos from timed pregnancies were stained for beta-galactosidase activity using standard methods. Briefly, embryos were fixed (1× PBS, 1% formaldehyde, 0.2% glutaraldehyde, 0.02% NP40) on ice for 2 h followed by three 15 min, room temperature washes (1× PBS, 2 mM $MgCl_2$, 0.02% NP40). Staining (1× PBS, 12 mM K-Ferricyanide, 12 mM K-Ferrocyanide, 0.002% NP40, 4 mM $MgCl_2$, and 320μg/ml 5-bromo-4-chloro-3-indolyl-b-D-galactopyranoside in *N*,*N*-dimethyl formamide) was carried out overnight at 37°C followed by two 30 min, room temperature washes (1× PBS, 0.2% NP40). Embryos were transferred to a final fixative solution (4% formaldehyde, 10% methanol, 100 mM sodium phosphate) for analysis and storage.

### Whole-mount *in situ* hybridization

Mouse embryos were fixed overnight in 4% paraformaldehyde in PBS. Reverse-transcribed digoxigenin-conjugated probes were made from linearized plasmids. *In situ* hybridizations were performed by using published protocols (60) with the following modifications. After probe hybridization, Ribonuclease A digestion was omitted, and Tris-buffered saline was used in place of PBS. BM-purple substrate (Roche, Molecular Biochemicals) was used in place of 5-bromo-4-chloro-3-indolyl phosphate/nitroblue tetrazolium. *Mitf* and *Si* cDNA containing plasmids (G370008D06Rik and G370069C13Rik, respectively) were first digested with Kpn1 and then transcribed with T3 polymerase to generate DIG-labeled *in situ* probes.

### Skin grafting

Skin grafting was performed according to standard procedures. Briefly, skin was grafted from late gestation embryos (approximately E16.5) onto 8–10 weeks old immune-compromised recipient mice (Albino Swiss Nude from Taconic; NTac:NIHS-*Foxn1*$^{nu/nu}$). Full-thickness skin grafts (∼1 cm in diameter) were removed aseptically from the dorsum of euthanized embryos and placed onto a similar sized dorsal skin excision made in the nu/nu recipient mice. The grafts were sutured into place and treated with triple antibiotic ointment three times per day for the first week following surgery. The grafts were allowed to grow until hair was apparent (3–4 weeks after initial surgery). Surgery and euthanasia protocols were performed in accordance with NHGRI ACUC guidelines.

## SUPPLEMENTARY MATERIAL

Supplementary Material is available at HMG Online.

## ACKNOWLEDGEMENTS

Andrew Salinger and Monica Justice (Baylor College of Medicine) provided assistance establishing our ENU injection protocol. Michael Wegner (Friedrich-Alexander University of Erlangen and Nuremberg, Erlangen, Germany) provided *Sox10*$^{LacZ}$ mice and Ulrich Ruther (Heinrich-Heine University, Düsseldorf, Germany) and Matthew Kelley (NIDCD, NIH) provided *Gli3*$^{D699}$ mice. Genotyping services used for mapping were provided by David Beier and Jennifer Moran (Brigham Women's Hospital, Harvard University), MaryPat Jones (NHGRI Genomics Core), and the Center for Inherited Disease Research (CIDR). Leslie Biesecker, Yingzi Yang, Doris Wu, and members of the Pavan laboratory provided helpful discussions and critical reading of the manuscript. Julia Fekecs provided graphic assistance.

*Conflict of Interest statement*. The authors have no competing interests.

## FUNDING

Genotyping costs were partially funded through the Mutation Mapping and Developmental Analysis Project (MMDAP) (NICHD grant U01 HD43430 to David Beier). CIDR is fully funded through a federal contract from the National Institutes of Health to The Johns Hopkins University, contract number N01-HG-65403. This research was supported in part by the Intramural Research Program of the National Human Genome Research Institute, National Institutes of Health (USA).

## REFERENCES

1. Baldwin, C.T., Hoth, C.F., Amos, J.A., da-Silva, E.O. and Milunsky, A. (1992) An exonic mutation in the HuP2 paired domain gene causes Waardenburg's syndrome. *Nature*, **355**, 637–638.
2. Bondurand, N., Dastot-Le Moal, F., Stanchina, L., Collot, N., Baral, V., Marlin, S., Attie-Bitach, T., Giurgea, I., Skopinski, L., Reardon, W. *et al.* (2007) Deletions at the SOX10 gene locus cause Waardenburg syndrome types 2 and 4. *Am. J. Hum. Genet.*, **81**, 1169–1185.
3. Tassabehji, M., Read, A.P., Newton, V.E., Harris, R., Balling, R., Gruss, P. and Strachan, T. (1992) Waardenburg's syndrome patients have mutations in the human homologue of the Pax-3 paired box gene. *Nature*, **355**, 635–636.
4. Tassabehji, M., Newton, V.E. and Read, A.P. (1994) Waardenburg syndrome type 2 caused by mutations in the human microphthalmia (MITF) gene. *Nat. Genet.*, **8**, 251–255.
5. Sanchez-Martin, M., Rodriguez-Garcia, A., Perez-Losada, J., Sagrera, A., Read, A.P. and Sanchez-Garcia, I. (2002) SLUG (SNAI2) deletions in patients with Waardenburg disease. *Hum. Mol. Genet.*, **11**, 3231–3236.
6. Puffenberger, E.G., Hosoda, K., Washington, S.S., Nakao, K., deWit, D., Yanagisawa, M. and Chakravart, A. (1994) A missense mutation of the endothelin-B receptor gene in multigenic Hirschsprung's disease. *Cell*, **79**, 1257–1266.
7. Hofstra, R.M., Osinga, J., Tan-Sindhunata, G., Wu, Y., Kamsteeg, E.J., Stulp, R.P., van Ravenswaaij-Arts, C., Majoor-Krakauer, D., Angrist, M., Chakravarti, A. *et al.* (1996) A homozygous mutation in the EDN3 gene associated with a combined Waardenburg type 2 and Hirschsprung phenotype (Shah-Waardenburg syndrome). *Nat. Genet.*, **12**, 445–447.
8. Edery, P., Attie, T., Amiel, J., Pelet, A., Eng, C., Hofstra, R.M., Martelli, H., Bidaud, C., Munnich, A. and Lyonnet, S. (1996) Mutation of the endothelin-3 gene in the Waardenburg-Hirschsprung disease (Shah-Waardenburg syndrome). *Nat. Genet.*, **12**, 442–444.

9. Pingault, V., Bondurand, N., Kuhlbrodt, K., Goerich, D.E., Prehu, M.O., Puliti, A., Herbarth, B., Hermans-Borgmeyer, I., Legius, E., Matthijs, G. *et al.* (1998) SOX10 mutations in patients with Waardenburg-Hirschsprung disease. *Nat. Genet.*, **18**, 171–173.
10. Mollaaghababa, R. and Pavan, W.J. (2003) The importance of having your SOX on: role of SOX10 in the development of neural crest-derived melanocytes and glia. *Oncogene*, **22**, 3024–3034.
11. Silver, D.L., Hou, L. and Pavan, W.J. (2006) The genetic regulation of pigment cell development. *Adv. Exp. Med. Biol.*, **589**, 155–169.
12. Southard-Smith, E.M., Kos, L. and Pavan, W.J. (1998) Sox10 mutation disrupts neural crest development in Dom Hirschsprung mouse model. *Nat. Genet.*, **18**, 60–64.
13. Britsch, S., Goerich, D.E., Riethmacher, D., Peirano, R.I., Rossner, M., Nave, K.A., Birchmeier, C. and Wegner, M. (2001) The transcription factor Sox10 is a key regulator of peripheral glial development. *Genes Dev.*, **15**, 66–78.
14. Tachibana, M., Kobayashi, Y. and Matsushima, Y. (2003) Mouse models for four types of Waardenburg syndrome. *Pigment Cell Res.*, **16**, 448–454.
15. Johnson, D.R. (1967) Extra-toes: anew mutant gene causing multiple abnormalities in the mouse. *J. Embryol. Exp. Morphol.*, **17**, 543–581.
16. Dickie, M.M. (1967) Presumed recurrences of mutations. *Mouse News Lett.*, **36**, 60.
17. Kang, S., Graham, J.M., Jr, Olney, A.H. and Biesecker, L.G. (1997) GLI3 frameshift mutations cause autosomal dominant Pallister-Hall syndrome. *Nat. Genet.*, **15**, 266–268.
18. Vortkamp, A., Gessler, M. and Grzeschik, K.H. (1991) GLI3 zinc-finger gene interrupted by translocations in Greig syndrome families. *Nature*, **352**, 539–540.
19. Johnston, J.J., Olivos-Glander, I., Killoran, C., Elson, E., Turner, J.T., Peters, K.F., Abbott, M.H., Aughton, D.J., Aylsworth, A.S., Bamshad, M.J. *et al.* (2005) Molecular and clinical analyses of Greig cephalopolysyndactyly and Pallister-Hall syndromes: robust phenotype prediction from the type and position of GLI3 mutations. *Am. J. Hum. Genet.*, **76**, 609–622.
20. Hui, C.C. and Joyner, A.L. (1993) A mouse model of Greig cephalopolysyndactyly syndrome: the extra-toesJ mutation contains an intragenic deletion of the Gli3 gene. *Nat. Genet.*, **3**, 241–246.
21. Pavan, W.J. and Tilghman, S.M. (1994) Piebald lethal (sl) acts early to disrupt the development of neural crest-derived melanocytes. *Proc. Natl Acad. Sci. USA*, **91**, 7159–7163.
22. Mackenzie, M.A., Jordan, S.A., Budd, P.S. and Jackson, I.J. (1997) Activation of the receptor tyrosine kinase Kit is required for the proliferation of melanoblasts in the mouse embryo. *Dev. Biol.*, **192**, 99–107.
23. Hakami, R.M., Hou, L., Baxter, L.L., Loftus, S.K., Southard-Smith, E.M., Incao, A., Cheng, J. and Pavan, W.J. (2006) Genetic evidence does not support direct regulation of EDNRB by SOX10 in migratory neural crest and the melanocyte lineage. *Mech. Dev.*, **123**, 124–134.
24. Rash, B.G. and Grove, E.A. (2007) Patterning the dorsal telencephalon: a role for sonic hedgehog? *J. Neurosci.*, **27**, 11595–11603.
25. Jiao, Z., Zhang, Z.G., Hornyak, T.J., Hozeska, A., Zhang, R.L., Wang, Y., Wang, L., Roberts, C., Strickland, F.M. and Chopp, M. (2006) Dopachrome tautomerase (Dct) regulates neural progenitor cell proliferation. *Dev. Biol.*, **296**, 396–408.
26. Wang, B., Fallon, J.F. and Beachy, P.A. (2000) Hedgehog-regulated processing of Gli3 produces an anterior/posterior repressor gradient in the developing vertebrate limb. *Cell*, **100**, 423–434.
27. Bose, J., Grotewold, L. and Ruther, U. (2002) Pallister-Hall syndrome phenotype in mice mutant for Gli3. *Hum. Mol. Genet.*, **11**, 1129–1135.
28. Flint, J., Valdar, W., Shifman, S. and Mott, R. (2005) Strategies for mapping and cloning quantitative trait genes in rodents. *Nat. Rev. Genet.*, **6**, 271–286.
29. Yang, H., Bell, T.A., Churchill, G.A. and Pardo-Manuel de Villena, F. (2007) On the subspecific origin of the laboratory mouse. *Nat. Genet.*, **39**, 1100–1107.
30. St Johnston, D. (2002) The art and design of genetic screens: *Drosophila melanogaster*. *Nat. Rev. Genet.*, **3**, 176–188.
31. Carpinelli, M.R., Hilton, D.J., Metcalf, D., Antonchuk, J.L., Hyland, C.D., Mifsud, S.L., Di Rago, L., Hilton, A.A., Willson, T.A., Roberts, A.W. *et al.* (2004) Suppressor screen in Mpl−/− mice: c-Myb mutation causes supraphysiological production of platelets in the absence of thrombopoietin signaling. *Proc. Natl Acad. Sci. USA*, **101**, 6553–6558.
32. Speca, D.J., Rabbee, N., Chihara, D., Speed, T.P. and Peterson, A.S. (2006) A genetic screen for behavioral mutations that perturb dopaminergic homeostasis in mice. *Genes Brain. Behav.*, **5**, 19–28.
33. Nadeau, J.H. and Frankel, W.N. (2000) The roads from phenotypic variation to gene discovery: mutagenesis versus QTLs. *Nat. Genet.*, **25**, 381–384.
34. Ruppert, J.M., Vogelstein, B., Arheden, K. and Kinzler, K.W. (1990) GLI3 encodes a 190-kilodalton protein with multiple regions of GLI similarity. *Mol. Cell. Biol.*, **10**, 5408–5415.
35. Ruiz i Altaba, A. (1999) Gli proteins and Hedgehog signaling: development and cancer. *Trends Genet.*, **15**, 418–425.
36. Lee, J., Platt, K.A., Censullo, P. and Ruiz i Altaba, A. (1997) Gli1 is a target of sonic hedgehog that induces ventral neural tube development. *Development*, **124**, 2537–2552.
37. Silver, D., Hou, L., Somerville, R., Young, M., Apte, S. and Pavan, W. (2008) The secreted metalloprotease ADAMTS20 is required for melanoblast survival. *PLoS Genet*, **4**, e1000003 doi:10.1371/journal.pgen.1000003.
38. Ruiz i Altaba, A., Nguyen, V. and Palma, V. (2003) The emergent design of the neural tube: prepattern, SHH morphogen and GLI code. *Curr. Opin. Genet. Dev.*, **13**, 513–521.
39. Biesecker, L.G. (2006) What you can learn from one gene: GLI3. *J. Med. Genet.*, **43**, 465–469.
40. Potterf, S.B., Furumura, M., Dunn, K.J., Arnheiter, H. and Pavan, W.J. (2000) Transcription factor hierarchy in Waardenburg syndrome: regulation of MITF expression by SOX10 and PAX3. *Hum. Genet.*, **107**, 1–6.
41. Lee, M., Goodall, J., Verastegui, C., Ballotti, R. and Goding, C.R. (2000) Direct regulation of the Microphthalmia promoter by Sox10 links Waardenburg-Shah syndrome (WS4)-associated hypopigmentation and deafness to WS2. *J. Biol. Chem.*, **275**, 37978–37983.
42. Bondurand, N., Pingault, V., Goerich, D.E., Lemort, N., Sock, E., Le Caignec, C., Wegner, M. and Goossens, M. (2000) Interaction among SOX10, PAX3 and MITF, three genes altered in Waardenburg syndrome. *Hum. Mol. Genet.*, **9**, 1907–1917.
43. Verastegui, C., Bille, K., Ortonne, J.P. and Ballotti, R. (2000) Regulation of the microphthalmia-associated transcription factor gene by the Waardenburg syndrome type 4 gene, SOX10. *J. Biol. Chem.*, **275**, 30757–30760.
44. Werner, T., Hammer, A., Wahlbuhl, M., Bosl, M.R. and Wegner, M. (2007) Multiple conserved regulatory elements with overlapping functions determine Sox10 expression in mouse embryogenesis. *Nucleic Acids Res.*, **35**, 6526–6538.
45. Aoki, Y., Saint-Germain, N., Gyda, M., Magner-Fink, E., Lee, Y.H., Credidio, C. and Saint-Jeannet, J.P. (2003) Sox10 regulates the development of neural crest-derived melanocytes in Xenopus. *Dev. Biol.*, **259**, 19–33.
46. Alvarez-Medina, R., Cayuso, J., Okubo, T., Takada, S. and Marti, E. (2008) Wnt canonical pathway restricts graded Shh/Gli patterning activity through the regulation of Gli3 expression. *Development*, **135**, 237–247.
47. Ulloa, F., Itasaki, N. and Briscoe, J. (2007) Inhibitory Gli3 activity negatively regulates Wnt/beta-catenin signaling. *Curr. Biol.*, **17**, 545–550.
48. Dunn, K.J., Brady, M., Ochsenbauer-Jambor, C., Snyder, S., Incao, A. and Pavan, W.J. (2005) WNT1 and WNT3a promote expansion of melanocytes through distinct modes of action. *Pigment Cell Res.*, **18**, 167–180.
49. Hari, L., Brault, V., Kleber, M., Lee, H.Y., Ille, F., Leimeroth, R., Paratore, C., Suter, U., Kemler, R. and Sommer, L. (2002) Lineage-specific requirements of beta-catenin in neural crest development. *J. Cell. Biol.*, **159**, 867–880.
50. Jin, E.J., Erickson, C.A., Takada, S. and Burrus, L.W. (2001) Wnt and BMP signaling govern lineage segregation of melanocytes in the avian embryo. *Dev. Biol.*, **233**, 22–37.
51. Takeda, K., Yasumoto, K., Takada, R., Takada, S., Watanabe, K., Udono, T., Saito, H., Takahashi, K. and Shibahara, S. (2000) Induction of melanocyte-specific microphthalmia-associated transcription factor by Wnt-3a. *J. Biol. Chem.*, **275**, 14013–14016.
52. Dorsky, R.I., Moon, R.T. and Raible, D.W. (1998) Control of neural crest cell fate by the Wnt signalling pathway. *Nature*, **396**, 370–373.
53. Dorsky, R.I., Raible, D.W. and Moon, R.T. (2000) Direct regulation of nacre, a zebrafish MITF homolog required for pigment cell formation, by the Wnt pathway. *Genes Dev.*, **14**, 158–162.

54. Saito, H., Yasumoto, K., Takeda, K., Takahashi, K., Yamamoto, H. and Shibahara, S. (2003) Microphthalmia-associated transcription factor in the Wnt signaling pathway. *Pigment Cell Res.*, **16**, 261–265.
55. Dorsky, R.I., Moon, R.T. and Raible, D.W. (2000) Environmental signals and cell fate specification in premigratory neural crest. *Bioessays*, **22**, 708–716.
56. Jeong, J., Mao, J., Tenzen, T., Kottmann, A.H. and McMahon, A.P. (2004) Hedgehog signaling in the neural crest cells regulates the patterning and growth of facial primordia. *Genes Dev.*, **18**, 937–951.
57. Ignatius, M.S., Moose, H.E., El-Hodiri, H.M. and Henion, P.D. (2007) Colgate/hdac1 repression of foxd3 expression is required to permit mitfa-dependent melanogenesis. *Dev. Biol.*, **313**, 568–583.
58. Justice, M. (2000) Mutagenesis of the mouse germline. In Jackson, I.J. and Abbott, C.M. (eds), *Mouse Genetics and Transgenics: A Practical Approach*. Oxford University Press, Oxford, UK, pp. 185–214.
59. Silver, L. (1995) Classical linkage analysis and mapping panels. In *Mouse Genetics: Concepts and Applications*. Oxford University Press, UK.
60. Wilkinson, D.G. and Nieto, M.A. (1993). In Wassarman, P. and DePamphilis, M. (eds), *Methods in Enzymology: Guide to Techniques in Mouse Development*. Academic, San Diego, pp. 361–373.
61. Selicorni, A., Guerneri, S., Ratti, A. and Pizzuti, A. (2002) Cytogenetic mapping of a novel locus for type II Waardenburg syndrome. *Hum. Genet.*, **110**, 64–67.
62. Southard-Smith, E.M., Angrist, M., Ellison, J.S., Agarwala, R., Baxevanis, A.D., Chakravarti, A. and Pavan, W.J. (1999) The Sox10(Dom) mouse: modeling the genetic variation of Waardenburg-Shah (WS4) syndrome. *Genome Res.*, **9**, 215–225.
63. Rhim, H., Dunn, K.J., Aronzon, A., Mac, S., Cheng, M., Lamoreux, M.L., Tilghman, S.M. and Pavan, W.J. (2000) Spatially restricted hypopigmentation associated with an Ednrbs-modifying locus on mouse chromosome 10. *Genome Res.*, **10**, 17–29.
64. Dai, P., Akimaru, H., Tanaka, Y., Maekawa, T., Nakafuku, M. and Ishii, S. (1999) Sonic Hedgehog-induced activation of the Gli1 promoter is mediated by GLI3. *J. Biol. Chem.*, **274**, 8143–8152.
65. Kalff-Suske, M., Wild, A., Topp, J., Wessling, M., Jacobsen, E.M., Bornholdt, D., Engel, H., Heuer, H., Aalfs, C.M., Ausems, M.G. *et al.* (1999) Point mutations throughout the GLI3 gene cause Greig cephalopolysyndactyly syndrome. *Hum. Mol. Genet.*, **8**, 1769–1777.
66. Zhou, H., Kim, S., Ishii, S. and Boyer, T.G. (2006) Mediator modulates Gli3-dependent Sonic hedgehog signaling. *Mol. Cell. Biol.*, **26**, 8667–8682.